VELOCITY MAPPING OF TURBULENT WAKES OF HYPERSONIC SPHERES WITH ARRAYS OF ION PROBE PAIRS

L. Sevigny, et al

Defence Research Establishment

Prepared for:

Advanced Research Projects Agency
Army Missile Command

August 1972

DREV R-663/72
PROJ. 95-51-10

NON CLASSIFIE
UNCLASSIFIED

VELOCITY MAPPING OF TURBULENT WAKES OF HYPERSONIC SPHERES WITH ARRAYS OF ION PROBE PAIRS

L. Sévigny, D. Heckman, A. Emond

CENTRE DE RECHERCHES POUR LA DEFENSE
DEFENCE RESEARCH ESTABLISHMENT
VALCARTIER

DEFENCE RESEARCH BOARD
CONSEIL DE RECHERCHES POUR LA DÉFENSE

Québec, Canada
August/août 1972

R37

DREV R-663/72
PROJ. 95-51-10

VELOCITY MAPPING OF TURBULENT WAKES OF HYPERSONIC SPHERES WITH ARRAYS OF ION PROBE PAIRS

by

L. Sévigny, D. Heckman, A. Emond

This research was sponsored jointly by

The Defence Research Establishment
Valcartier
P.O. Box 990, Courcelette
Quebec, Canada

The Advanced Research Projects
Agency
ARPA Order 133
Monitored by the US Army
Missile Command
Redstone Arsenal
Alabama 35809
Contract DA-H01-69-C-0921

CENTRE DE RECHERCHES POUR LA DEFENSE
DEFENCE RESEARCH ESTABLISHMENT
VALCARTIER
Tel: (418) 844-4271

Québec, Canada

August/août 1972

RESUME

Le champ de vitesse du sillage d'une sphère hypersonique est déterminé à l'aide d'un double peigne transverse de sondes ioniques pouvant comporter jusqu'à huit paires de sondes. Les mesures ont porté sur des sillages d'une sphère en titane de 2.7 pouces de diamètre, lancée à 14 500 pieds à la seconde, dans un corridor de tir rempli d'azote. Deux pressions furent utilisées soit 7.6 et 20 torr. La vitesse de convection mesurée se compare harmonieusement avec la vitesse moyenne de sillage déduite de l'expérience des étincelles consécutives pour de l'air dans des conditions similaires. De plus, la technique des peignes de sondes a permis d'étendre la détermination du champ de vitesse au voisinage immédiat du projectile, ce qu'il n'est pas possible de faire à l'aide de la technique des étincelles consécutives par suite de la difficulté de former des étincelles distinctes dans cette région du proche sillage en raison du fort degré d'ionisation qui y règne.

En comparant les données obtenues à 7.6 et à 20 torr, on s'aperçoit que la valeur de la vitesse de convection le long de l'axe de vol augmente avec la pression. D'un autre côté, si l'on considère la largeur de sillage en vitesse on constate qu'elle est plus grande à basse pression, du moins dans le proche sillage. Au delà de 300 ou 400 diamètres de projectile, cependant, les données aux deux pressions étudiées ont tendance à se superposer. Ces observations semblent corroborer les informations provenant d'autres sources à l'effet que le sillage, à 7.6 torr de pression, d'une sphère de 2.7 pouces, n'est pas complètement turbulent avant 300 ou 400 diamètres de projectile.

ABSTRACT

The technique of measuring convection velocity in the hypersonic wake with a pair of in-line probes has been applied on a large scale to the mapping of the velocity field in the hypersonic wake through the use of a transverse survey array containing up to 8 ion-probe pairs. Measurements are reported of the velocity field in the wakes of 2.7 inch diameter spheres flown at 14,500 feet/second in ballistic range atmospheres at 7.6 torr and at 20 torr of nitrogen. The array technique leads to convection velocity results which are in excellent agreement with the mean wake velocity data obtained by the sequential spark technique in an air atmosphere. In addition, the technique has permitted an extension of the mapping of the velocity field of 15,000 feet/second spheres to considerably smaller axial distances than was possible with the spark method because of the difficulty to forming distinct sparks at the higher levels of ambient ionization encountered in the near wake.

A comparison of the data obtained at 7.6 torr and at 20 torr shows that the amplitude of the velocity distribution in the wake, as defined by the velocity on the wake axis, is higher at higher pressure. Considering the wake width however, it is found that the width of the velocity distribution is larger at the lower pressure of 7.6 torr than is the case at 20 torr, at least in the near wake. However, at axial distances greater than 300 or 400 diameters, the data for the two pressures tend to overlap. These observations appear to be related to other information indicating that for 2.7 inch diameter spheres launched at 7.6 torr, the wake is not fully turbulent until about 300 or 400 diameters.

TABLE OF CONTENTS

1.0 INTRODUCTION

The measurement in the turbulent wake of hypersonic projectiles of the axial and radial variation of the velocity distribution is of considerable interest for the development of turbulent mixing models for the wake. Such models of mixing, in combination with temperature data and reacting chemistry schemes, are required to predict the persistence of various chemical species in the wake (References 1, 2).

Recently systematic production of statistically significant quantities of spatially-resolved mean wake velocity data has been achieved using the sequential spark technique (References 3, 4). In the spark technique, a column of ionized gas is created along an arbitrary path across a wake, and the distortion of this path is subsequently recorded at known time intervals so that a displacement history and consequently a mean velocity estimate can be obtained. Both sphere and cone wakes have been studied over a wide range of ambient pressure and projectile velocity including both laminar and turbulent wake flows. One of the few limitations on the technique occurs when the ambient density is so low or the ionization in the wake is so high that an electrical discharge through the wake produces only a glow, rather than a well-defined spark path. For example, this limitation makes it impossible to measure a velocity profile across a sphere wake at axial distances less than about 300 body diameters for a 15,000 feet/second hypersonic sphere.

Another velocity-measuring technique can be devised for the ionized hypersonic wake by locating two electrostatic probes in the wake so that one is exactly downstream (or axially displaced) from the other, and measuring the time it takes for an ionized blob (or eddy) of fluid to travel or be convected the known distance between the two probes. As concerns their general applicability, such techniques employing two-or-more probes in axial configuration depend on the wake being turbulent; while they cannot produce velocity data at radial distances less than a body radius, they do permit velocity measurements just behind the projectile. Of course, being based on correlation methods, such techniques generally demand considerable computer effort. With a single pair of probes, data can only be obtained at one arbitrary value of radial distance on a given round, and consequently a large number of rounds are required to obtain reasonable statistics at any particular value of radial distance. Up to the present, rather limited quantities of convection velocity data have been reported from measurements with axial arrays of up to 5 electrostatic probes on large hypersonic sphere wakes (References 5, 6) and with pairs of hot wires or cooled film anemometers (References 7, 8) on supersonic sphere wakes.

The sequential spark technique is believed to measure a mean wake velocity. There is some reason to believe that wake convection velocity estimates may be different from the so-called mean wake velocity measurements obtained at the same location in the wake (References 8, 9, 10). However, the wake convection velocity data measured with pairs of probes have so far been found to be in general agreement with other wake velocity data.

The efficiency of the two-probe wake velocity measuring technique can be increased by using many pairs of probes distributed across the wake in a transverse survey array configuration. In the present paper we report on velocity measurements made in the wakes of 2.7 inch diameter spheres flown at 14,500 feet/second in the ballistic range facilities at the Defence Research Establishment Valcartier (DREV), using transverse survey arrays of electrostatic ion probe pairs.

2.0 EXPERIMENTAL TECHNIQUE

The basic ion probe pair consists of two separate cylindrical-type probes held in tandem fashion in a thin support about 12 inches in height (Figure 1). Each cylindrical probe consists of a 2 millimeter long segment of 0.28 millimeter diameter gold wire, formed by stripping the outer jacket and teflon insulator from miniature solid-jacketed coaxial cable to expose the center conductor. Probes are normally biased to collect ions; a compensating current is collected by the remaining jacket and by the support stem. When in use, each 2-probe pair is mounted in the range so that an imaginary line drawn between the tips of the two probes would be parallel to the axis of flight of the projectile. Up to eight such elemental 2-probe axial arrays are mounted together to form one so-called 'transverse survey array' (Figure 2). The separation between the collecting wires in an individual 2-probe element is 0.95 centimeter; as regards the direction of the mean flow, the second probe is directly in the shadow of the first probe. If the probes are spaced too tightly, erroneous estimates of wake velocity are obtained. Systematic investigation of the effect of probe diameter and probe spacing on the wake velocity estimate obtained with pairs of probes have been carried out by Ghosh and Richard (Reference 11), using a plasma jet facility. For probes of the size used in the present experiment, their results shows that underestimation occurs only for probe separations of less than 0.7 centimeter. Experiments at DREV using probe separations of 0.48 centimeter confirmed the existence of severe velocity underestimation effects for small probe separation. No such effects are believed to exist at the normal probe separation distance of 0.95 centimeter, because of two observations. The first of these is based on the results of Ghosh and Richard which indicate that even for probes of diameter up to 0.625 millimeter, considerably larger than those employed here, there is no effect as long as the separation distance is at least one centimeter. The second is the fact of the exceptionally close agreement of the present results with those obtained by the sequential spark experiment.

The eight 2-probe elements in the survey array are separated laterally by multiples of 1.25 inches. Both symmetrical and asymmetrical arrangements of probes (with respect to the flight axis) have been employed. The probe signals are fed from the probe tips into one of the 16 pre-amplifier box beneath or above the survey array. The shape of the pre-amplifier box was determined by considerations of minimization of the strength of the reflected bow shock wave system from structure in the hypersonic range. The range itself was the 10 foot inside diameter

hypersonic Range 5 facility, which consists of a 425 foot long evacuable free-flight facility along which various models can be flown (Reference 12). The actual free diameter of the range is reduced at the experimental station to slightly less than 5 feet by the presence of a smoothly-profiled fiberglas wedge treatment installed on the walls. This treatment has been found experimentally (Reference 13) to significantly attenuate the outgoing bow shock system originating with the projectile. If the range walls were not treated, the shock system would reflect at the walls and then collapse toward the axis of the tank; in the process, significant disturbance of wake measurements would be caused (Reference 14). The launcher itself is a light gas gun which routinely launches saboted models up to 4 inches in diameter at velocities of 14,500 feet/second. In the flight chamber, model attitude and position are routinely determined by a system of flash X-rays. This position data permits the determination of the flight axis of the projectile with respect to the probes. The probes are optically surveyed in place in the range before the launching.

The electrostatic survey arrays have normally been employed using saturation ion current collection, the probes being biased at minus 4 volts with respect to ground. (The plasma potential in the wake will be slightly positive with respect to ground). The bias is supplied by an operational type current-to-voltage preamplifier, which tends to neutralize probe capacitive effects and which drives the eight feet or so of coaxial cable needed to transmit the probe signals to the exterior of the range tank. The preamplifier employs a feedback resistor of 200 kilohms and has a response which is flat between dc and 200 kilohertz, falling smoothly off to -3 db between 200 and 400 kilohertz (Figure 3). The bias voltage is subtracted in a type 'O' unit, and the residual probe signal is amplified by a Hewlett Packard 467A dc power amplifier and delivered by means of 170 feet of terminated 92 ohm cable to the recording room. Recording is carried out by means of Tektronix 551 and 555 double beam oscilloscopes and Wollensak 35 millimeter Fastax cameras, which provide an effective sweep rate of about 200 microseconds/centimeter. For velocity measurements, each probe of a pair is recorded using one beam of the same oscilloscope; the two probe signals are recorded in synchronization. Timing marks are introduced by means of Z-modulation every millisecond, these assist in synchronization and film velocity measurement. Film velocity variation amounts to a fraction of 1% between adjacent 1 millisecond signal segments. Figures 4a and 4b show typical recordings of pairs of signals obtained with a survey array at pressures of 7.6 and 20 torr.

The convection-velocity-measuring technique using a pair of electrostatic ion probes to detect convected ionization fluctuations in the turbulent hypersonic wake has a rather large advantage compared to other applications of continuum-type electrostatic probes. As long as the probes detect a signal which is roughly proportional to the local ionization being swept past the probes, it is possible to neglect the problem of exactly interpreting the probe current in terms of charge density (Reference 15). In effect one is only interested in the time

delay occuring from the moment a given signal feature is seen on the upstream probe to the moment the same feature appears on the downstream probe. Of course, there may be many such features in a short signal segment, and one does not attempt to measure an average time delay directly. Instead the two signals from the probes are cross-correlated, and the resulting cross-correlation curve is used to provide the desired estimate of wake velocity (Reference 12).

3.0 ANALYSIS

The first stage in the analysis process is the digitalization of the analog signal traces recorded in pairs on 35 millimeter film. To read the film a 'positive' must be made, where the signal appears as a transparent trace on a black background. This positive is fed into an automatic or computer-controlled film reader assembled at DREV (Reference 16). In the reader a small spot of light is displayed on a precision CRT and then imaged onto the film. Collection optics behind the film directs the transmitted light to a photomultiplier tube. At the same time some light from the spot on the CRT is removed with a beam splitter, passed through similar optics and uniform density filter and measured with a second photomultiplier. The output signals of the two photomultipliers are compared, and the results of the comparison indicate whether the density of the particular spot on the film is more or less than the reference density. The results of the comparison are fed to a digital computer which controls the coordinates of the spot displayed and which is programmed so as to conditionally scan the film to locate and follow the signal trace. The digitalization of the signal trace is simply a consequence of the signal tracing process of the reader. The data is outputed on magnetic tape and subsequently printed out on a line printer by the XDS computer, at which stage any anomalies are spotted and control cards for analysis instructions are prepared.

The timing marks on the signal traces form a convenient common time reference for all the signal pairs recorded on a given round. The duration of the timing marks (about 10 microseconds) is short compared to the frequency content of the probe signals; the reader simply interpolates across the gap in the trace but flags the points at the same time. The reading frequency normally employed is about 450-500 kilohertz, so that the 4 or 5 consecutive flagged points appearing every 500 points are readily recognized as timing marks. By means of trigger, delay units, and calibrated high-sweep-speed oscilloscopic recording, it is possible to relate certain features on the film traces to the time at which the projectile passed the measuring station and consequently fix the time of occurrence of the reference timing marks with respect to the time of passage of the projectile. The timing marks also permit the synchronization in time of the signals recorded from a pair of probes.

Several considerations enter into the choice of the length (in time) of the signal samples which are cross-correlated during the velocity estimating process (Figures 4, 5). Decay of the charge density in the wake and slowdown in the wake velocity as functions of time or, equivalently, distance behind the projectile introduce respectively nonstationarity in the amplitude and in the frequency content of the random current signals detected by the electrostatic probes. The signals can be rendered quasi-stationary by considering sufficiently short segments of signal. On the one hand, it is preferable to have a short signal in order to more precisely localize the region of the wake where the velocity estimate is made; on the other hand the result is more precisely estimated from a statistical point of view if the length of the samples which are being cross-correlated can be increased. With large projectiles such as the 2.7 inch diameter spheres being fired at DREV, the variation of probe signal amplitude and wake velocity are considerably slower in time than that experienced with smaller models, and it has been found convenient to use signal segment lengths of 0.5 millisecond duration. The segments are chosen to begin or to end on the timing marks; there are two individual segments defined between any pair of consecutive timing marks. For 2.7 inch diameter spheres flying at 14,500 feet/second, the projectile recedes from the measuring station at about 66 diameters/millisecond, equivalently the effective axial distance behind the projectile over which an individual 0.5 millisecond signal segment is correlated varies by about 33 body diameters. At axial distances greater than about 100 diameters this axial distance variation is barely significant. The velocity estimate is attributed to the mid-point of the signal segment or, more exactly, to the axial distance behind the projectile corresponding to the value of time at this point. For axial distances at which the normalized local wake velocity to projectile velocity ratio has dropped to 0.1, the actual length of the (0.5 millisecond) sample of wake convected past the probes and over which the cross-correlation function is evaluated is about 3 diameters; correspondingly, when the ratio drops to 0.01, the length of wake involved is only about half a diameter.

Theoretically one would argue that the convection velocity measured by a pair of probes is an 'averaged' velocity. In practice, because one feature in a probe signal may dominate other features and consequently the cross-correlation function, the velocity estimates obtained by such a pair of probes frequently tend to be more like instantaneous estimates of wake velocity parallel to the flight axis, rather than average values. It is well to point out here that measurements made in a wake by a stationary probe in the range as the wake flows past and over the probe are transient-type measurements. The whole measurement is over in about 10 to 30 milliseconds. This is in considerable contrast to the case of the study of a steady-state jet, where the probes can be inserted at a given fixed distance from the throat of the jet and measurements made until the cross-correlation function is as well averaged as the experimenter requires. Because of the considerable tendency of the present 2-probe velocity estimates towards 'instantaneous' velocity estimates, there is reason to believe that the rms velocity fluctuation data derived from the distribution of velocity data points obtained by the present technique may be considerably closer to the true value than might otherwise be believed.

Certain data-handling problems were encountered with the transverse survey array technique which were not apparent when measuring velocity with the equivalent of a single pair of probes. In effect, the survey array of eight 2-probe velocity-measuring elements allows axial velocity history profiles to be obtained at roughly 8 independent positions or radial distances on the same round. Data is generated at about 8 times the rate possible with a single pair of probes. In the process of analysis, 200 or more cross-correlation functions and their associated velocity estimates are generated.

Figure 5 illustrates a typical cross-correlation function curve P_1P_2, generated from two sampled probe signals which have been correlated. Each discrete point on such a curve is computed for an integer number of lags $n\Delta t$, where n is an integer and Δt is the sampling interval used in digitalization of the probe signals. Now the appropriate time lag which corresponds to the time for a given ionized eddy to travel between a pair of probes is characterized not by the time T_m at which the cross-correlation function P_1P_2 has its maximum, but rather by the time T_t corresponding to the point where the envelope LL' is tangent to the curve P_1P_2 (Reference 9). A computer program was written in order to find this point of tangency automatically, here the envelope LL' is approximated by a straight line. The algorithm employed was based on a simple observation: if a,b are the coordinates of a computed point of the correlation, then the line passing from the point (0,1) to the point (a, b) has a slope equal to

$$M = (b-1)a.$$

If $|M|$ is plotted as a function of T, the resulting curve will have a minimum at the point of tangency. Before being put into general application, the program was thoroughly tested on a round which had already been analyzed manually by finding the point where the envelope appeared to be tangent to the computed and plotted curve. Only rarely did the differences in the results obtained by the computer and by an experienced technician vary by more than 5%. The principal source of error in the determination of an individual velocity estimate probably resides in the approximation of the curve for the envelope by a straight line. It is difficult to evaluate if the error introduced is systematic; one thing that can be said with certainty is that this error is negligible by comparison with the scattering of the results observed because of the statistical nature of the turbulence-driven fluctuations in the velocity estimates.

Once velocity data becomes available from a number of rounds, it becomes of interest to attempt to estimate the mean character of the velocity distribution in the wake and the character of the velocity fluctuations. The data to be considered in this paper have been obtained by observations on about 15 firings of 2.7 inch diameter spheres at 14,500 feet/second in an atmosphere of 7.6 torr nitrogen and roughly half that number of firings at 20 torr nitrogen. Because of the Reynolds number or $P_\infty D$ dependence of wake velocity (Reference 17), the two sets of data have been analyzed separately. The number of data points in each set is

considerable. For example, the fifteen rounds fired at 7.6 torr furnish, for various values of the radial distance parameter R/D and for values of the axial distance X/D behind the projectile extending from 0 to about 1500 diameters, roughly 1200 independent spatially-resolved or point estimates of convection velocity. The approach adopted in order to deal with this data consisted of dividing the results into sets corresponding to various bands of axial distances behind the projectile. The data in each band was fitted by a biparametric gaussian distribution of the form

$$\frac{V}{V_\infty} = \frac{V_o}{V_\infty} \exp\left(-\frac{R^2}{r^2}\right),$$

where the least mean squares method is used to find the amplitude and the width of the distribution. These two parameters, respectively V_o/V_∞ and r/D, represent the ratios of the axial velocity of convection to the velocity of the projectile, and of the convection velocity radius of the wake to the diameter of the projectile. The adequacy of the gaussian distribution for such curve fitting has been established for wake velocity by the spark technique (References 4, 17). One of the practical questions that should be faced in fitting this distribution is that of deciding what should be the widths of the bands of axial distance that define the number of data points in a given set.

Several considerations enter into the choice of a suitable width for the axial distance bands which contain the sets of points used to define the gaussian fits. One can define a lower limit on the basis of the following argument. Each point measurement of velocity obtained with a survey array has associated two coordinates: a radial distance R/D, which is essentially exact, and an axial distance behind the projectile X/D, which is imprecise by about ± 16, based on the fact that the basic correlation interval is 0.5 milliseconds or 32 body diameters. It would be futile to attempt to use bands narrower than 32 diameters for the simple reason that the narrower the band, the fewer the number of data points in the set.

It is important to realize that one of the parameters that is established by the fit is the axial value of the convection velocity. For physical reasons, it is impossible to get closer to the wake axis with a pairs of probes than a radial distance of 0.5 diameter; most of the data corresponds to radial distance values greater than 0.8 diameter. In order to increase the statistical precision of the gaussian fit to the velocity data, it is desirable to utilize the largest possible set of data points, without sacrificing too much the axial resolution of the measurements.

One can ask the question as to whether there exists some optimum bandwidth which would reconcile both, precision and resolution. The question has been tackled experimentally on the XDS computer using the actual experimental data. Figure 6a shows a comparison of calculations of axial velocity using three different bandwidths. In the first case

(open triangles), the width was chosen to be 100 diameters with no overlap between adjacent bands. In the second case (open circles) the width of the band was 30 diameters plus an overlap of 15 diameters at each end for a total width of 60 diameters. Finally in the third and last case (solid circles) the total width of the band was 30 diameters with no overlap. As is evident from Figure 6a, the three different bandwidths give practically the same results, thus indicating that within certain limits, the width of the bands has little influence on the profile of convection velocity as a function of axial distance. Similar findings were made with regard to the radius of the velocity wake (Figure 6b).

4.0 RESULTS

A typical radial profile of convection velocity derived from a 60 diameter band of data centered at 420 diameters behind a sphere is shown in Figure 7. The curve passing through the data is gaussian, having an amplitude on the wake axis $V_o/V_\infty = 0.05$, and a radius $r/D = 2.28$. The full circles indicate the mean values obtained by averaging all the data points in radial sectors of width 0.2 diameter taken consecutively across the wake. All data on the figure has been normalized by the value of the normalized wake velocity on the axis (V_o/V_∞). Figure 7 illustrates well certain features common to all such radial velocity profiles. One notes that the velocity estimates are not uniformly distributed as a function of R/D: there are none at values of R/D less than 0.8, and very few corresponding to radial distances greater than the apparent profiles radius (here $r/D = 2.28$). This has the result that the wake radius is not very well determined, particularly at larger axial distances behind the projectile. However, there are enough data points in the vicinity of the wake axis to ensure that the axial value of the assumed gaussian distribution of velocity is determinable with acceptable precision.

Quantitatively, the precision of the derived parameters V_o/V_∞ and r/D can be displayed with the aid of contours of levels of confidence. Figure 8 shows four such confidence contours encircling a point (indicated by a cross) whose coordinates are the amplitude and width parameters of the gaussian curve in Figure 7. The 'percentage' attached to each contour of the figure indicates the probability that the true values of V_o/V_∞ and r/D are enclosed within that contour. We have chosen somewhat arbitrarily to use confidence contours at 90% in order to specify the precision attached to the results of the radial profile curve-fitting. Rather than associate a 'contour' to each fit, it is simpler to give only the outer limits of the projection of these confidence contours on the axes. In other words, one can specify the dimensions of the circumscribing rectangle. These limits of confidence are considered to be relatively conservative. For example, the specification of a confidence level of 90% is equivalent, in the case of a gaussian error curve, to specifying error limits at $\pm 1.64\ \sigma$, where σ is the standard deviation.

The behavior of the velocity on the axis of the wake behind a 2.7 inch diameter sphere flown at 14,500 feet/second in a 7.6 torr nitrogen atmosphere, previously given in Figure 6, is plotted again in Figure 9a with the 90% confidence limits added on certain points. Horizontal error limits are also given; these correspond to the previously-mentioned imprecision of ± 16 diameters in the value of the axial distance to which a convection velocity estimate belongs. Figure 9a shows the behavior with axial distance of the radius of the velocity profile of the wake deduced simultaneously with the behavior of the velocity on the wake axis. (Appendix A furnishes tabulations of both the wake velocity on the axis and the wake radius as a function of axial distance from 2.7 inch sphere firings at 7.6 torr, for several bandwidths).

Figures 10a and 10b present data similar to that shown in Figure 9 in that they give respectively wake velocity on the axis and the velocity radius of the wake as a function of axial distance, except that here the ambient pressure in the range was 20 torr nitrogen. (The data are tabulated in Appendix B).

The data of Figure 9 for firings in 7.6 torr nitrogen atmosphere and of Figure 10 for firings at 20 torr, are plotted together in Figure 11. Consider first the behavior of the wake convection velocity along the axis of the wake. One notes that the profile corresponding to 7.6 torr ($P_\infty D$ = 20 torr-inches) falls below that corresponding to 20 torr ($P_\infty D$ = 54 torr-inches). The difference between the two profiles is systematic and statistically significant, and the direction of the difference indicates that an increase in ambient pressure entails an increase in wake velocity. Also shown on Figure 11a are several extremely precise estimates of the mean wake velocity on the axis determined by Lahaye et al. (Reference 4) and Lahaye (Reference 17) using the sequential spark technique (and 15,000 feet/second spherical projectiles launched in air atmospheres). These data were obtained under experimental conditions similar to those described here except that the diameter of the spherical projectiles used did not exceed one inch. Obviously, the spark results agree very well with those obtained using arrays of probes, despite any difference in atmospheric composition. One concludes that the array measurements confirm the spark data, and that there is no difference between the probe convection velocity and the mean wake velocity. Additionally, the probe array technique has permitted a mapping of the wake velocity field in the region of axial distance less than 300 diameters behind the spheres. As is indicated by the straight line of slope -1 on the graph, the decay of the wake convection velocity on the axis follows a power law of minus unity, for axial distances X/D between 300 and 1000 diameters.

Concerning the velocity radius of the wake, as has been previously discussed, the present array techniques have not permitted us to determine the wake radius with precision. In effect, the problem is attributable in large measure to a distribution of the measurements over radial distance which does not lend itself to wake width determination. Relative to the size of the wake, the individual velocity estimates are

grouped too near to the wake axis, especially at large axial distances (such as 1000 diameters). This being recognized, it still remains the fact that in Figure 11b there appears to be a difference in the size of the wake velocity width at 7.6 torr and the size of the wake at 20 torr, for axial distances X/D less than 300 or 400 diameters. Contrastingly, for axial distances greater than 400 diameters, the size of the wake seems to be identical for the two pressures. However, if we examine the results of the sequential spark technique, at X/D = 300, we find that these data indicate a much weaker dependence of the width of the wake on the ambient pressure than is indicated by the data obtained using axial array.

The environment in which a hypersonic wake develops is characterized by very strong variations in density (Reference 18) as contrasted with the constant density environment of a low speed projectile wake. In the description of flow fields, the effects of variable density or compressibility can often be removed by a coordinate transformation, that of Howarth-Dorodnitsyn, which becomes in the axisymmetric case

$$(R_{HD}/D)^2 \quad 2\int_0^{R/D} \frac{\rho}{\rho_\infty} y\,dy,$$

where R_{HD}/D represents the transformed coordinate normalized to the projectile diameter and where

R/D is the radial position in the laboratory coordinate system,
ρ is the wake density
ρ_∞ is the density at free stream
y is a dummy variable of integration.

Through the use of the Howarth-Dorodnitsyn transformation one might expect to suppress the effect of compressibility on the radial profiles of convection velocity, thereby affecting slightly the deduced axial velocity and more strongly the width of the velocity wake, so that these would tend to behave in the same fashion as for a low speed wake. The density data required to carry out the transformation is available from measurements carried out at DREV on the wakes of 2.7 inch diameter spheres flown at 14,500 feet/second in a 7.6 torr nitrogen atmosphere, and recently published in the proceedings of a NATO Specialist's Conference on turbulent shear flows (Reference 19).

The Howarth-Dorodnitsyn transformation was originally applied only to compressible laminar flows; however, Laufer (Reference 20) has shown that it can be equally applied to compressible turbulent flows. Figure 12 presents a simple graph permitting one to calculate the Howarth-Dorodnitsyn radius for a 2.7 inch diameter sphere at 14,500 feet/second in 7.6 torr nitrogen. As one can see the modification introduced by this coordinate transformation is far from negligible. For example at an axial distance of 100 diameters, a velocity estimate obtained at R/D = 2 is displaced to R_{HD}/D = 1 after the transformation.

The axial profile of convection velocity on the wake axis in the transformed coordinate system as well as the transformed wake velocity width are shown in Figure 13. These curves have been obtained by fitting the transformed radial velocity data with a least mean squares routine, exactly as was previously done on the untransformed data. The remarkable fact concerning the two profiles of Figure 13 is that they apparently follow the asymptotic laws for turbulent wakes, i.e. a decay of - 2/3 for the velocity on the wake axis and a growth law of + 1/3 for the wake width. The points in the region of axial distance of 1000 diameters depart from the general trend, however. It should be pointed out that these latter points are the least precise because of the small number of measurements available in this region.

Unfortunately, owing to the unavailability of density data for wakes at 20 torr it has not been possible to apply the transformation to the convection velocity data obtained at this pressure.

5.0 DISCUSSION

A comparison of the experimental measurements presented in the preceding section raises several questions of considerable importance. It will be recalled that the results concerning wake convection velocities were all obtained under practically the same experimental conditions, except for pressure, which alternated between 7.6 and 20 torr nitrogen. In all cases, the projectile consisted of a hollow titanium sphere of diameter 2.7 inches, flown at a velocity of approximately 14,500 feet/second. Figures 11a and 11b summarize graphically the influence of pressure on the behavior with axial distance of the convection velocity on the wake axis and of the width of the wake. One notes in the latter case a somewhat intriguing behavior. At the lower pressure (7.6 torr N_2) the size of the wake is relatively constant until about 700 diameters, after which distance the wake continues to grow but apparently in a disorganized fashion. Contrastingly, at higher pressure (20 torr N_2), the wake width begins to grow in the neighborhood of 200 diameters, apparently following a 1/3 power rate. Another curious feature is that for axial distances less than 300 or 400 diameters behind the projectile, the width of the velocity wake at 20 torr is smaller than that obtained at 7.6 torr. One can ask the question as to whether these differences are due to some qualitative differences between the turbulence at the two pressures or if possibly the differences have something to do with the laminar turbulent transition.

On the basis of schlieren studies (Reference 21) it appears that behind blunt bodies, transition occurs abruptly from straight laminar flow to well-developed turbulence within a few axial body diameters. In the case of the present measurements at 7.6 torr, the Reynolds number based on sphere diameter is about 2×10^5, and from the data of Wilson (Reference 21), the normalized transition data should be about 7 diameters behind the projectile. Thus the wake should be turbulent at the two

pressures considered in this paper. Nevertheless the behavior of the signals (Figure 4) tends to raise doubts as to the character of the turbulence exhibited by the wake at 7.6 torr, at least in the first 200 or 300 diameters. In the near wake (X/D < 100), the signals recorded at 7.6 torr contain very few fluctuations at high frequencies compared to the 20 torr signals; in fact, at 7.6 torr, high frequencies make their appearance only between 100 and 300 diameters. This observation is corroborated quantitatively by the relatively high number of estimates of very large space scales (larger than the sphere diameter) obtained in the near wake at 7.6 torr, whereas there are hardly any such at 20 torr (Reference 22).

It is apparent, then, that there are several well-defined differences in the observed behavior of the wake at 7.6 torr and at 20 torr. One could tend to conclude from these differences that the wake at 7.6 torr is transitionary in the region near to the projectile and does not become completely turbulent until about 300 diameters, thereby admitting a contradiction between the present results and those of Wilson. However, examination of Figure 13 leads us to reconsider this tentative conclusion. In effect, if one suppresses the effect of compressibility from the data at 7.6 torr by applying the coordinate transformation of Howarth-Dorodnitsyn, one obtains an axial behavior of the convection velocity measured on the wake axis and of the wake width which seems to conform to the asymptotic laws characteristic of low speed turbulent wakes. Thus on the basis of Figure 13, the wake of a sphere flown in a nitrogen atmosphere at 7.6 torr would become completely turbulent around 150 diameters and the turbulent flow would be self-similar. However, after Corrsin and Kistler (Reference 23), a minimum condition for self-similarity is that the ratio of the standard deviation of the instantaneous position of the turbulent front in the wake to the mean position must be constant. Measurements of intermittency at DREV indicate that between 100 and 400 diameters, this ratio can be represented by a straight line of positive slope (Reference 24).

As one can see, the interpretation of the results presented in this article is not an easy task. At the same time we have no doubt that these results conform well to physical reality.

6.0 CONCLUSION

The technique of measuring convection velocity in the hypersonic wake with a pair of in-line probes has been applied on a large scale to the mapping of the velocity field in the hypersonic wake through the use of a transverse survey array containing up to 8 ion-probe pairs. Measurements are reported of the velocity field in the wakes of 2.7 inch diameter spheres flown at 14,500 feet/second in ballistic range atmospheres at 7.6 torr and at 20 torr in nitrogen. The array technique leads to convection velocity results which are in excellent agreement with the mean wake velocity data obtained by the sequential spark technique in an air atmosphere. In addition, the technique has permitted an extension of the

mapping of the velocity field of 14,500 feet/second spheres to considerably smaller axial distances than was possible with the spark method because of the difficulty of forming sparks at the higher levels of ambient ionization encountered in the near wake.

A comparison of the data obtained at 7.6 torr and at 20 torr shows that the amplitude of the velocity distribution in the wake, as defined by the velocity on the wake axis, is higher at higher pressure. Considering the wake width however, it is found that the width of the velocity distribution is larger at the lower pressure of 7.6 torr than is the case at 20 torr, at least in the near wake. However, at axial distances greater than 300 or 400 diameters, the data for the two pressures tend to overlap. These and other observations on the wakes at 7.6 and 20 torr tend to indicate that the wake behind a 2.7 inch diameter sphere at 7.6 torr may not be completely turbulent before 300 or 400 diameters behind the projectile.

ACKNOWLEDGEMENT

The authors are grateful to Mr. F. Caron who carried out the correlation analysis of the probe signals and are deeply indebted for the technical assistance of Messrs G. Moisan and D. Audet as well as Miss C. Proulx and Miss N. Bérubé.

Preceding page blank

REFERENCES

1. Lykoudis, P., "A review of hypersonic wake studies", RAND/RM - 4493 ARPA, 1965 (Unclassified), also AIAA Journal, Vol. 4, No. 4, pp. 577-590, April 1966.

2. Zeiberg, S.L. and Bleich, G.D., "Finite-difference calculation of hypersonic wakes", AIAA Journal, Vol. 2, No. 8, pp. 1396-1402, August 1964.

3. Lahaye, C., Léger, E.G. and Lemay, A., "Wake velocity measurements using a sequence of sparks", AIAA Journal, Vol. 5, No. 12, pp. 2274-2276, December 1967.

4. Lahaye, C., Jean, L. and Doyle, H., "Velocity distributions in the wake of spheres", AIAA Journal, Vol. 8, No. 8, pp. 1521-1527, August 1970.

5. Kirkpatrick, A., Heckman, D. and Cantin, A., "Wake plasma turbulence study using an electrostatic probe array", AIAA Journal, Vol. 5, No. 8, pp. 1494-1495, August 1967.

6. Heckman, D., Cantin, A., Emond, A. and Kirkpatrick, A., "Convection velocity measurements in hypersonic sphere wakes", AIAA Journal, Vol. 6, No. 4, pp. 750-752, April 1968.

7. Fox, J., "Space correlation measurements in the fluctuating turbulent wakes behind projectiles", AIAA Journal, Vol. 6, No. 2, pp. 270-276, February 1971.

8. Fox, J. and Rungaldier, H., "Anemometer measurements of velocity and density in projectile wakes", AIAA Journal, Vol. 9, No. 2, pp. 270-276, February 1971.

9. Fisher, H.J. and Davies, P.O.A.L., "Correlation measurements in a non-frozen pattern of turbulence", Journal Fluid Mechanics, Vol. 18, pp. 97-116, January 1964.

10. Lumley, J.L., "The interpretation of time spectra measured in high-intensity shear flows", Physics of Fluids, Vol. 8, No. 6, pp. 1056-1062, June 1965.

11. Ghosh, A.K. and Richard, C., "Probe geometry effect on turbulent plasma diagnostics", RCA Victor Company Ltd., Research Laboratories Report No. 3.900.12, May 1968.

12. Heckman, D., Tardif, L. and Lahaye, C., "Experimental study of turbulent wakes in the CARDE free-flight ranges", Proceedings of the Symposium on Turbulence of Fluids and Plasmas, Microwave Research Institute Symposium Series, Vol. XVIII, Polytechnic Press, (distributed by Interscience), 1969.

13. Heckman, D., Dionne, J.G.G., Lahaye, C., Moir, L., Podesto, B., Robertson, W. and Williams, J., "On minimizing the effects of reflected shocks in ballistic ranges", (to be published).

14. Heckman, D., Lahaye, C., Moir, L., Podesto, B. and Robertson, W., "A shock wave treatment for ballistic ranges", AIAA Journal, Vol. 8, No. 7., pp. 1355-1357, July 1970.

15. Cantin, A., Emond, A. and Heckman, D., "Observations on electrostatic probe behavior in collision-dominated ionized turbulent gas flows in ballistic ranges", ICIASF'69 Record of the 3rd International Congress on Instrumentation in Aerospace Simulation Facilities, pp. 20-33, May 1969.

16. Holland, J.H., and Galbraith, D.S., "A computer-controlled film reader", Proceedings of the Third Data Processing Seminar held at Defence Research Establishment Suffield, May 10-12, 1967, compiled by R.B. Harvey, DRES, March 1968.

17. Lahaye, C., "Velocity distributions in sphere wakes", DREV R 682 (Unclassified) (to be published).

18. Dionne, J.G.G. and Tardif, L., "An application of the electron beam fluorescence probe in hyperballistic range wake studies", ICIASF'71 Record of the 4th International Congress on Instrumentation in Aerospace Simulation Facilities, pp. 80-86, June 1971.

19. Dionne, J.G.G., Heckman, D., Lahaye, C., Sévigny, L. and Tardif, L., "Fluid dynamic properties of turbulent wakes of hypersonic spheres", presented at the AGARD Fluid Dynamics Panel Specialist's Meeting on "Turbulent Shear Flows", held in London 13-15 September 1971, and published in the AGARD Conference Proceedings.

20. Laufer, J., "On turbulent shear flows of variable density", Memorandum RM-5549-ARPA, May 1968.

21. Wilson, L.N., "Body-shape effects on axisymmetric wakes: Transition", AIAA Journal, Vol. 4, No. 10, pp. 1741-1747, October 1966.

22. Sévigny, L. and Heckman, D., under preparation.

23. Corrsin, S. and Kistler, A.L., "Free-stream boundaries of turbulent flows", NACA Report 1244 (1955).

24. Heckman, D. and Sévigny, L., "Structure of turbulent wakes of hypersonic sphere as inferred with ion probes", DREV R 669, (Unclassified) (to be published).

FIGURE 1

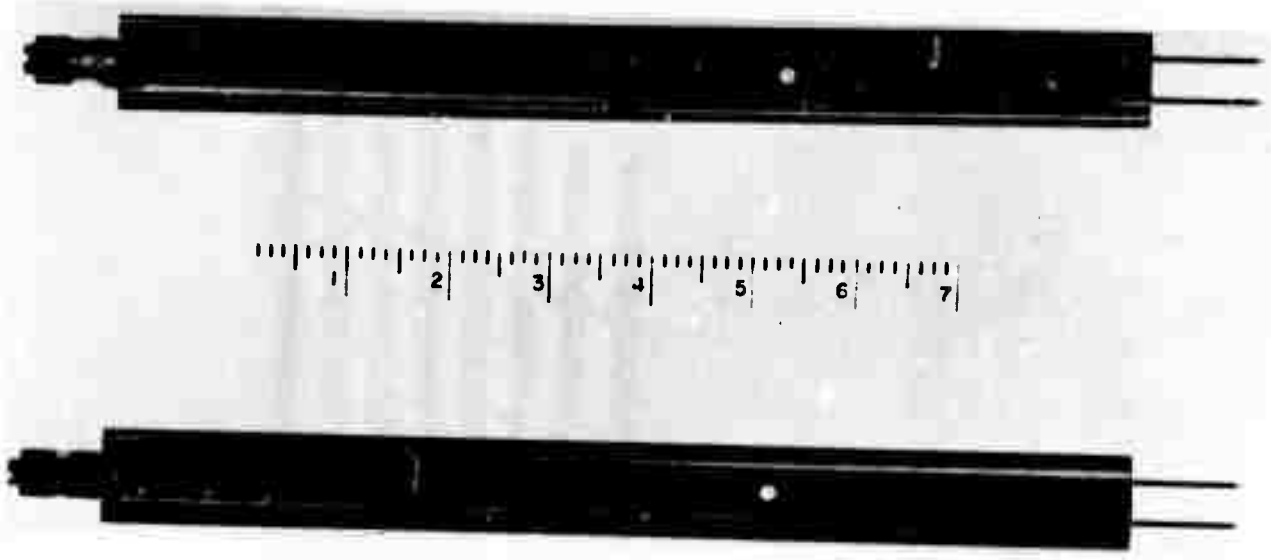

FIGURE 2

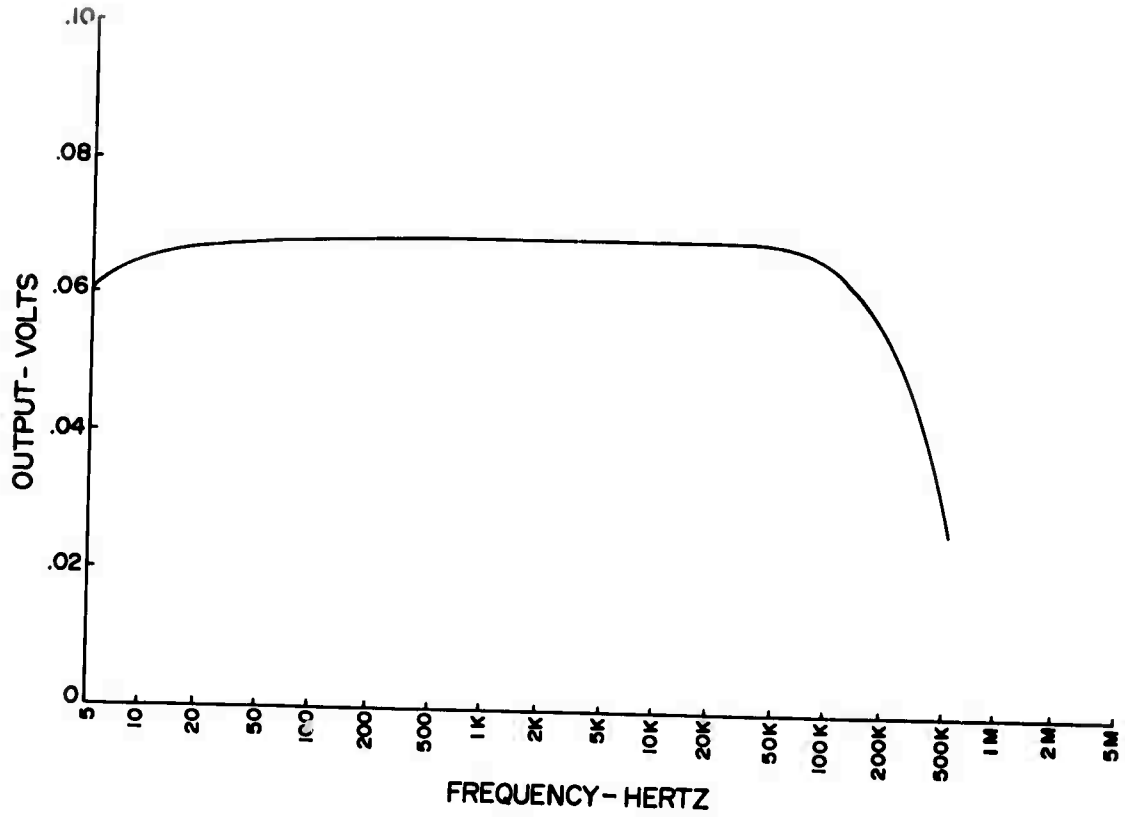

FIGURE 3

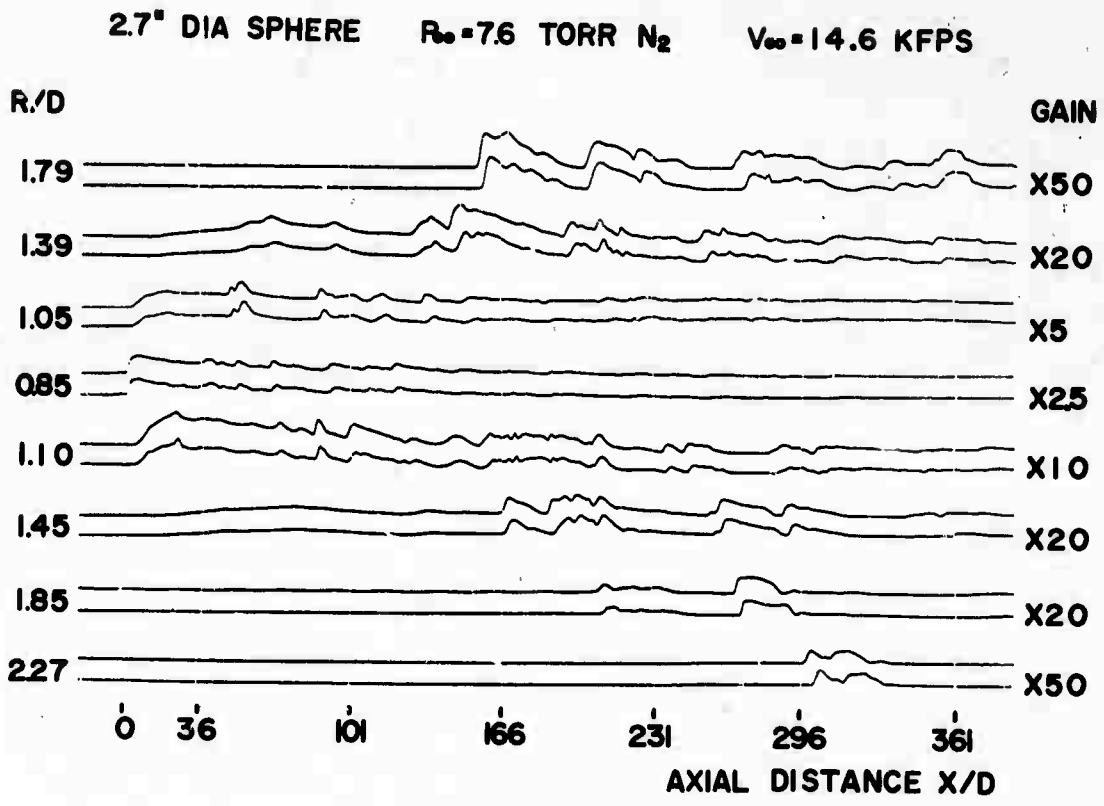

FIGURE 4a

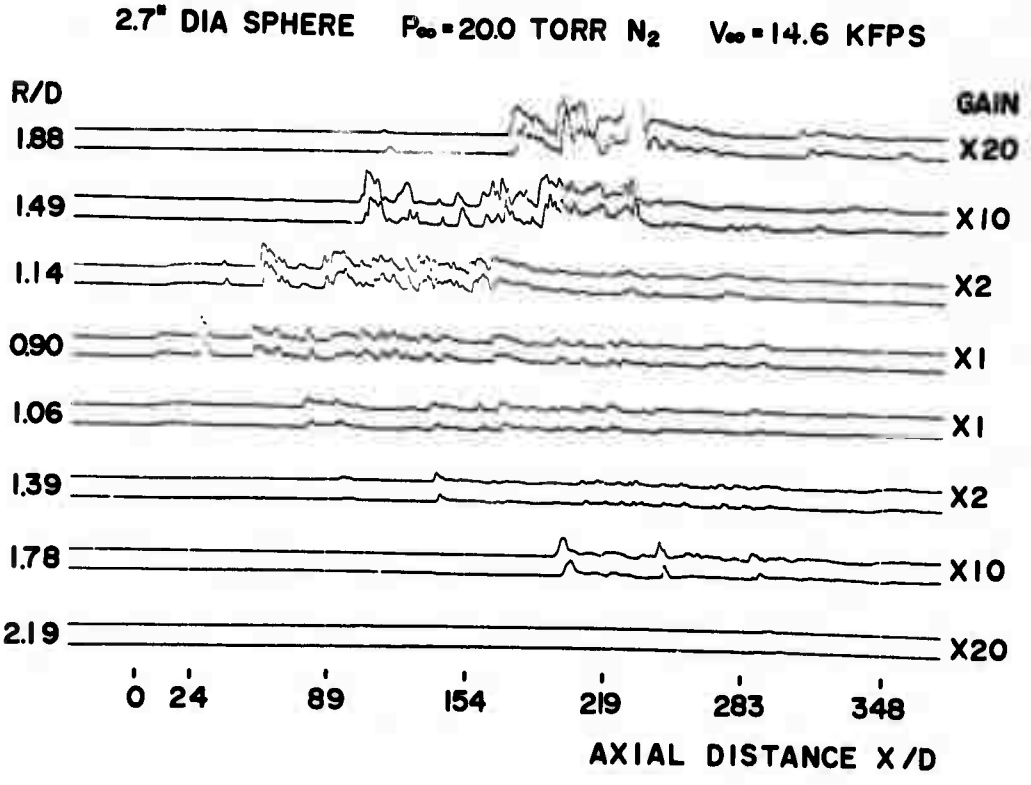

FIGURE 4b

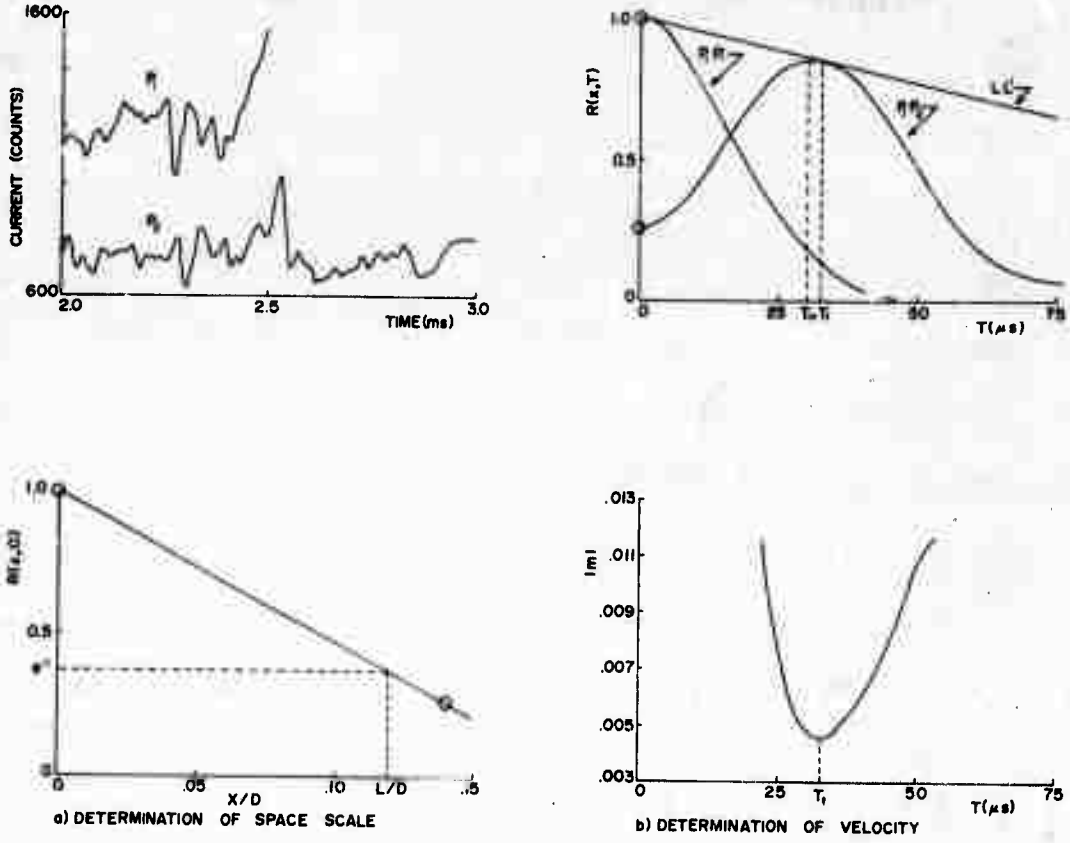
1600
600
CURRENT (COUNTS)
2.0
2.5
3.0
TIME(ms)
1.0
0.5
0
R(s,T)
RR
LL
RR
T(μs)
1.0
0.5
0
.05
.10
L/D
.5
X/D
a) DETERMINATION OF SPACE SCALE
.013
.011
.009
.007
.005
.003
Im I
0
25
50
75
T(μs)
b) DETERMINATION OF VELOCITY

FIGURE 5

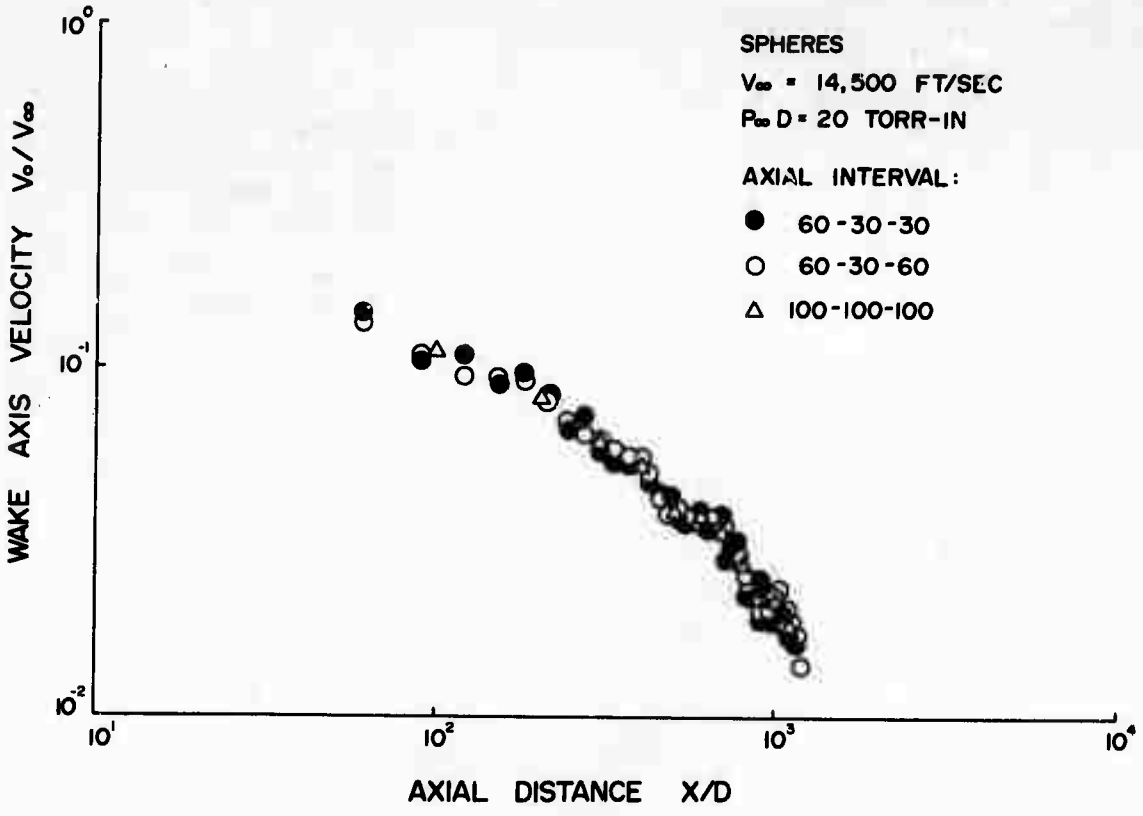

FIGURE 6a

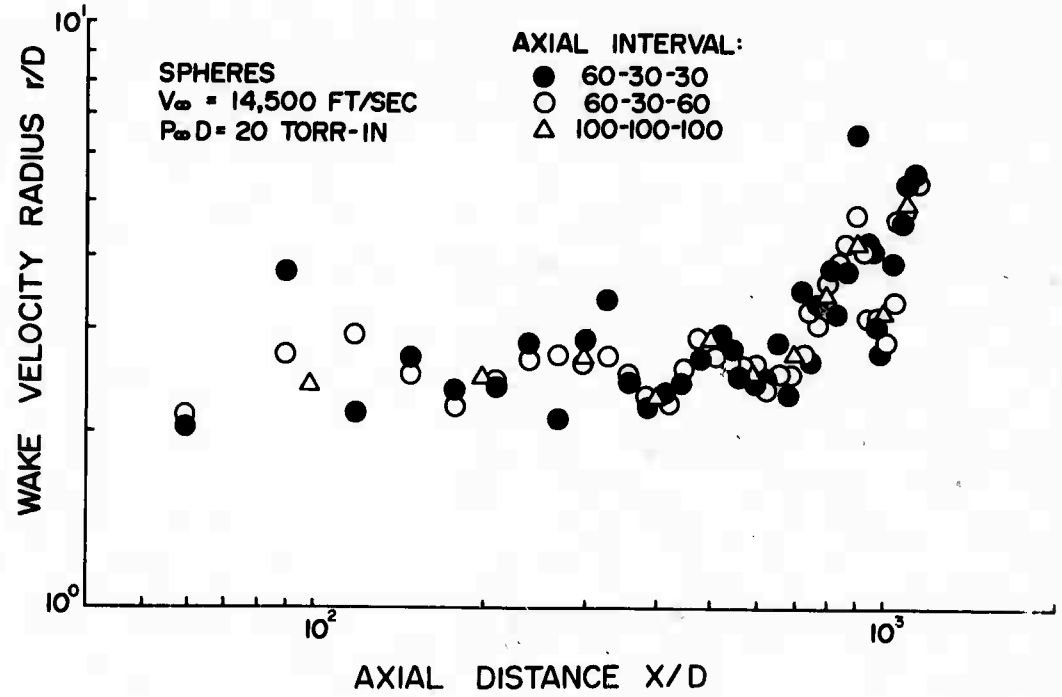

FIGURE 6b

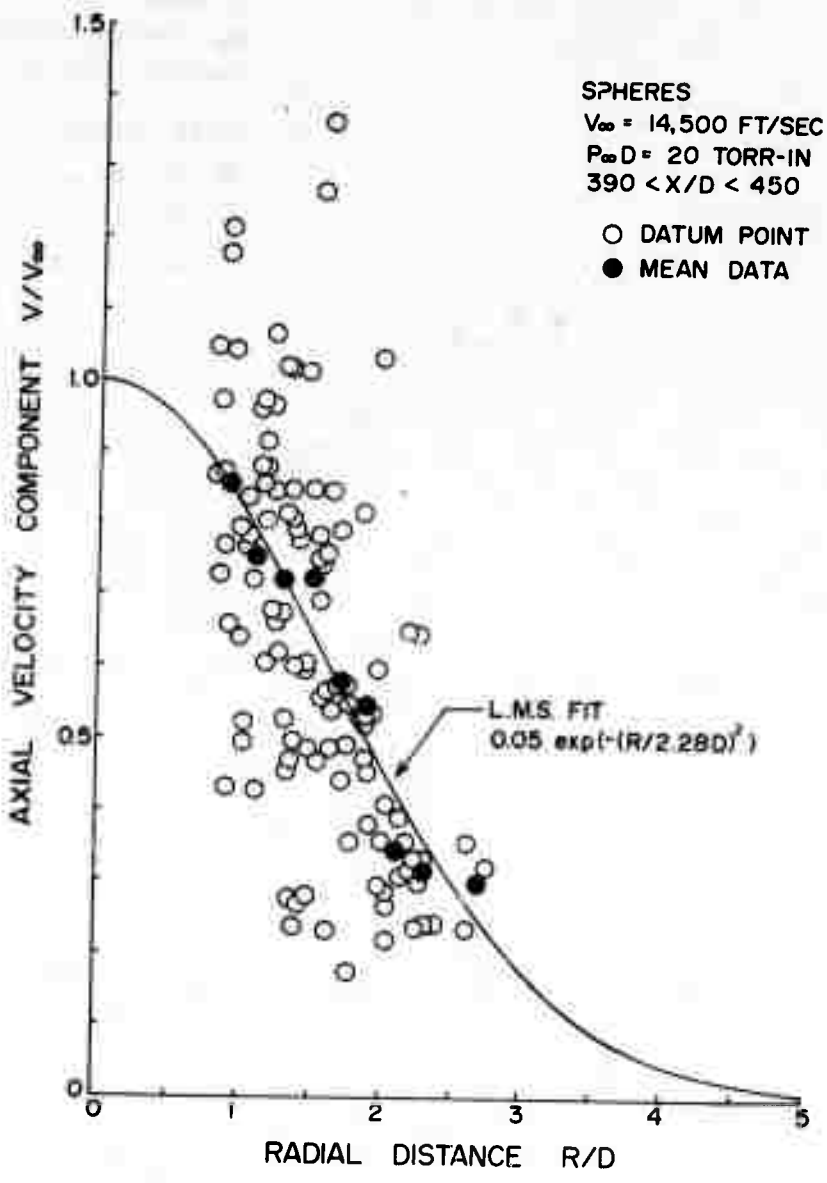
SPHERES
V∞ = 14,500 FT/SEC
P∞D = 20 TORR-IN
390 < X/D < 450
O DATUM POINT
● MEAN DATA
L.M.S. FIT
0.05 exp[-(R/2.280)²]
AXIAL VELOCITY COMPONENT V/V∞
RADIAL DISTANCE R/D
1.5
1.0
0.5
0
0
1
2
3
4
5

FIGURE 7

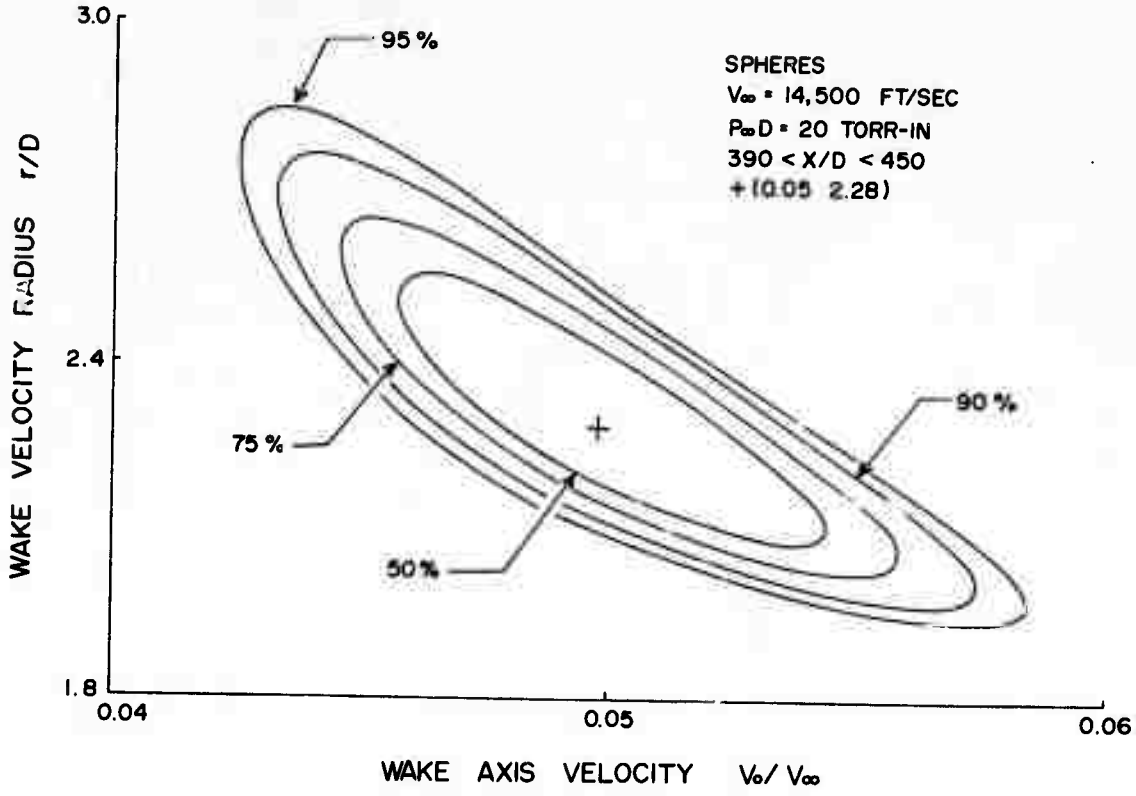
3.0
2.4
1.8
0.04
0.05
0.06
95 %
90 %
75 %
50 %
SPHERES
V∞ = 14,500 FT/SEC
P∞D = 20 TORR-IN
390 < X/D < 450
+ (0.05 2.28)
WAKE VELOCITY RADIUS r/D
WAKE AXIS VELOCITY V0/ V∞

FIGURE 8

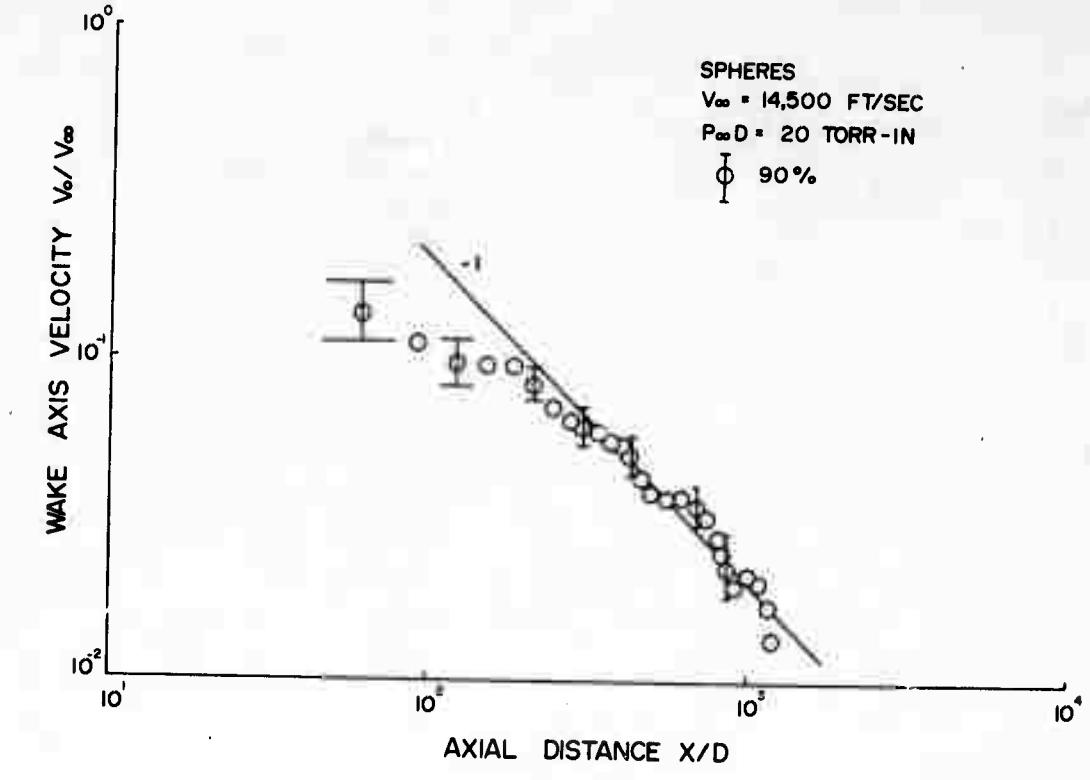

FIGURE 9a

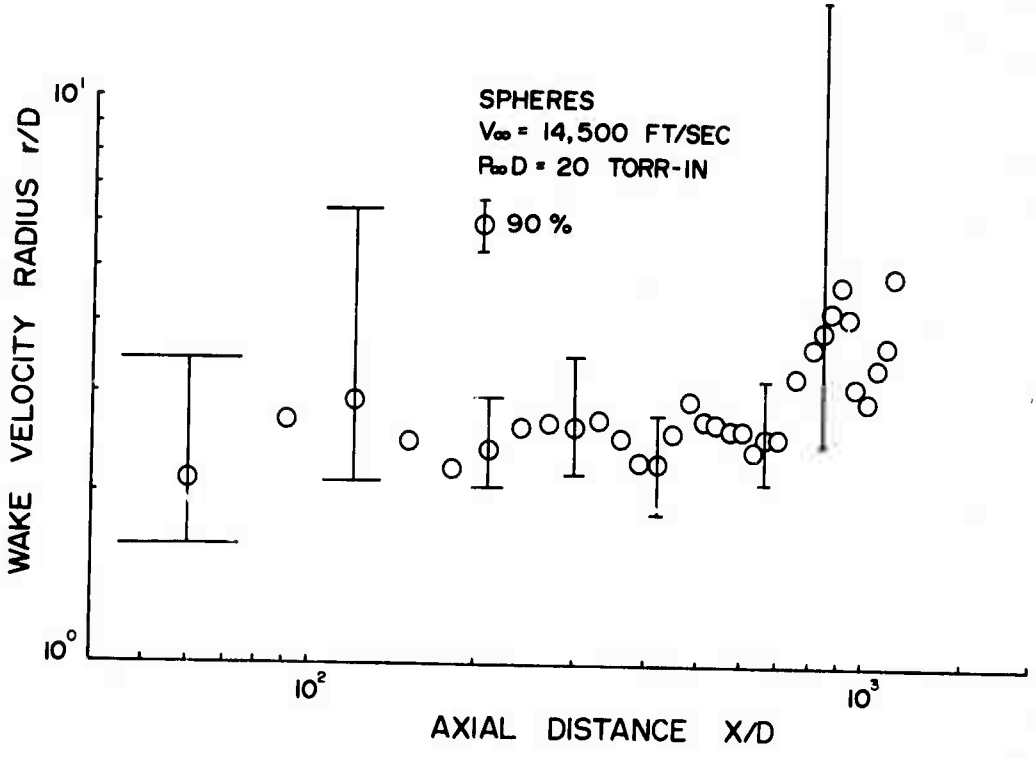

FIGURE 9b

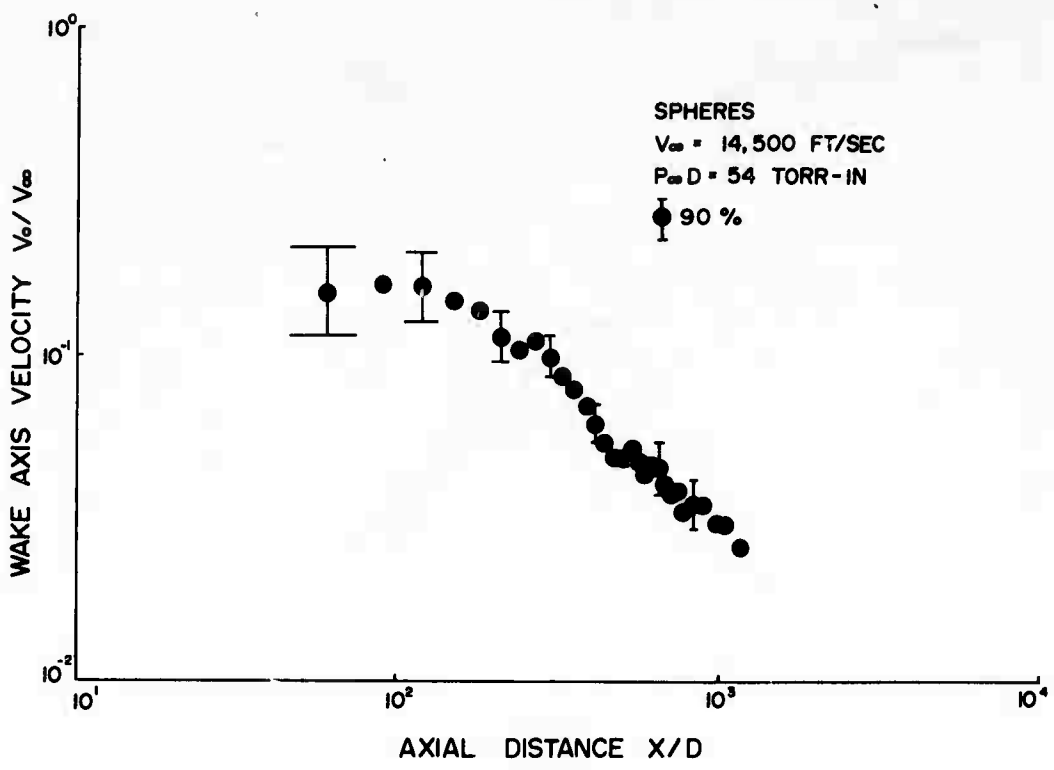

FIGURE 10a

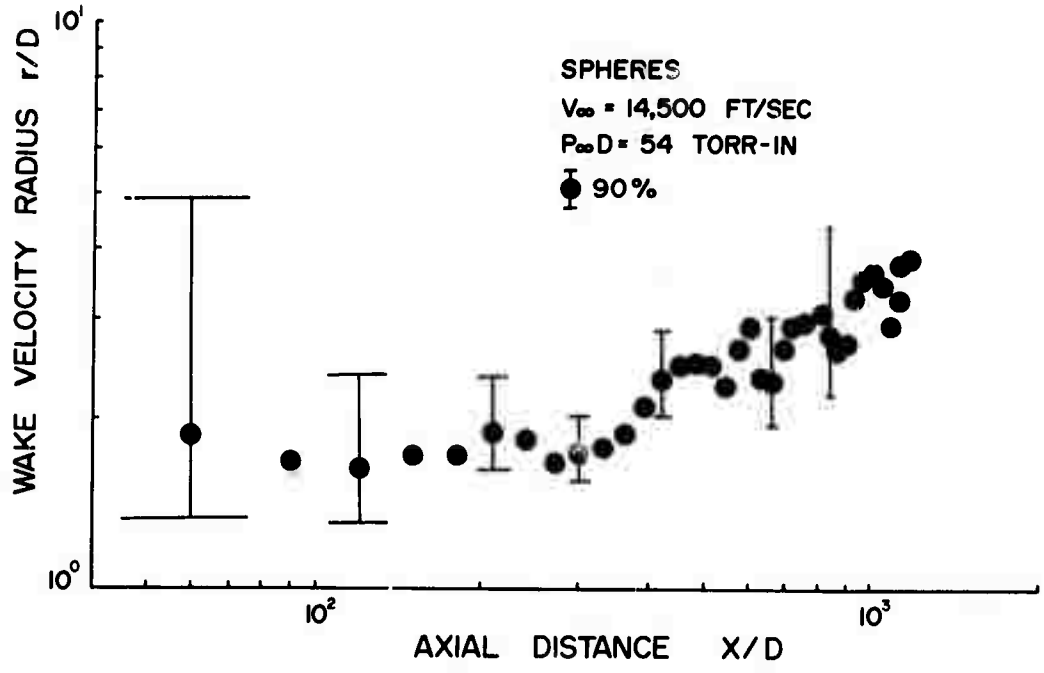

FIGURE 10b

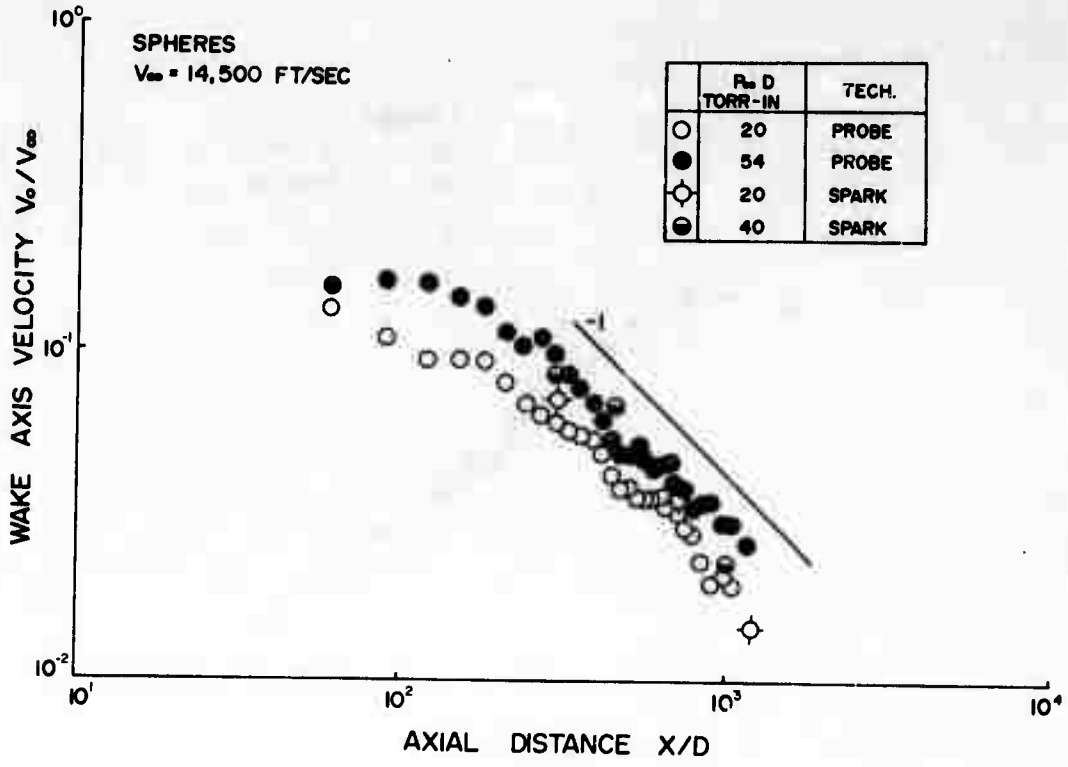

FIGURE 11a

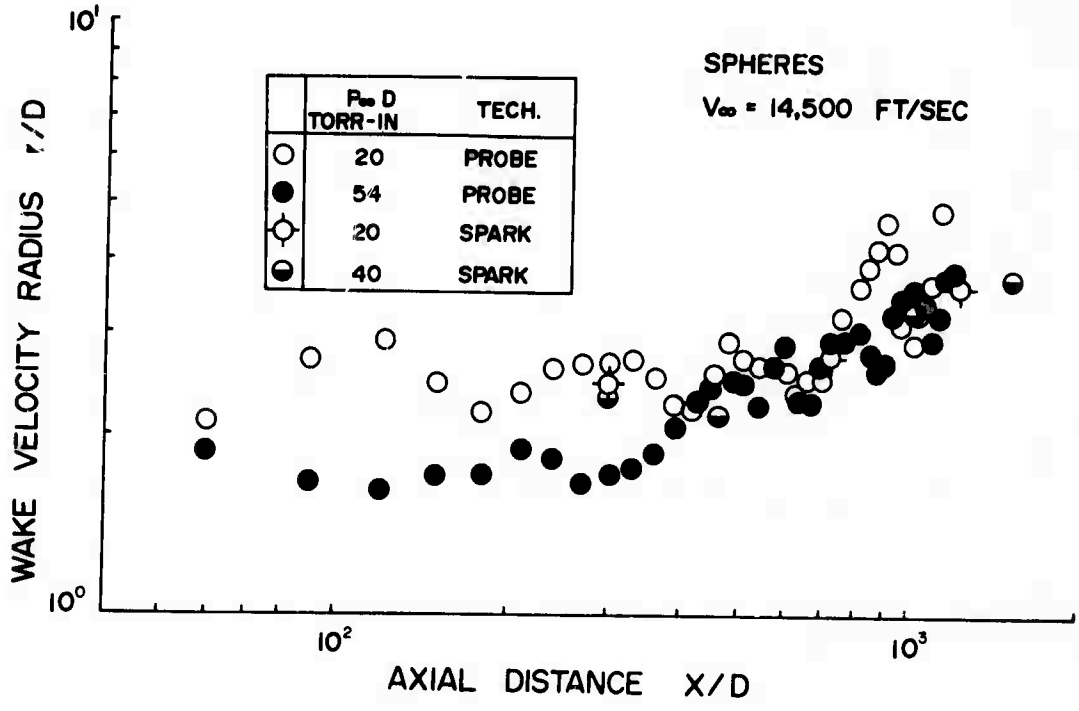

FIGURE 11b

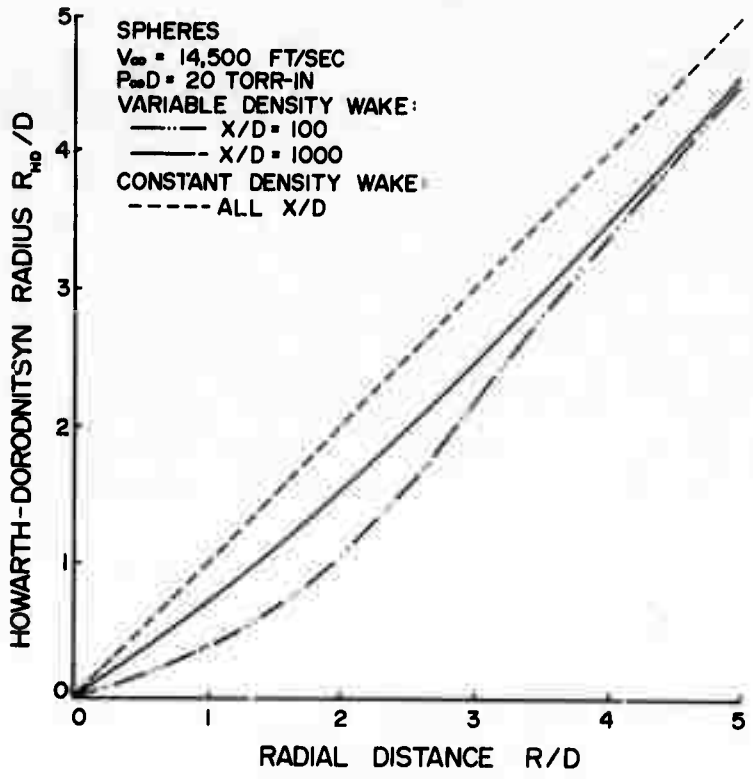

FIGURE 12

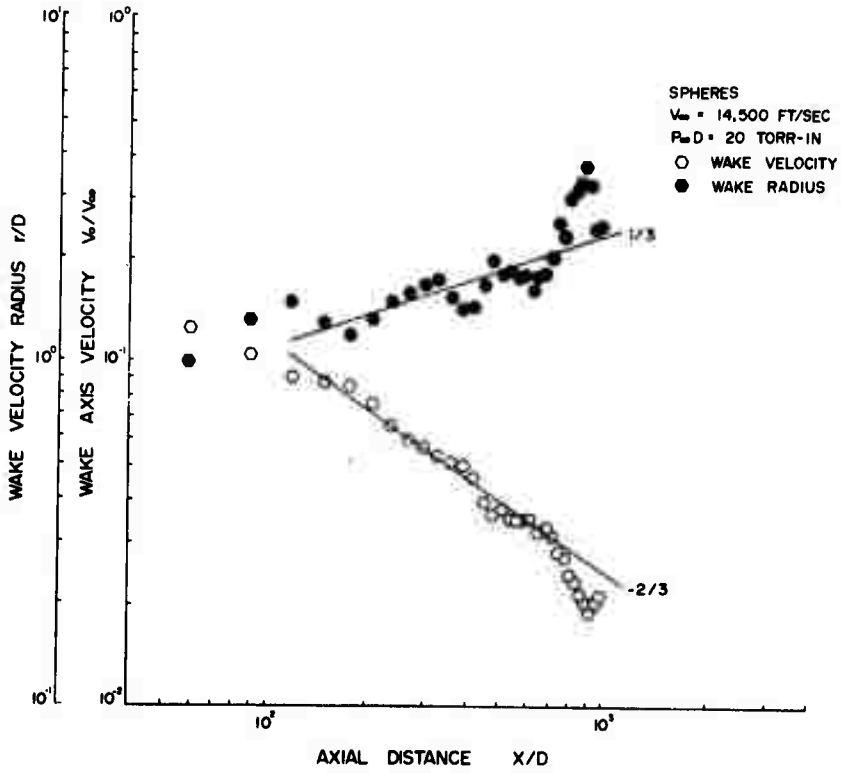

FIGURE 13

APPENDIX A

This appendix contains three tables giving all the pertinent numerical values pertaining to the fits of the radial profiles of the convection velocity at 7.6 torr (20 torr-inches). Each table is characterized by a three number combination (per example 60-30-60) describing the way the axial bands are built. The first number designates the axial coordinate of the center of the first band, the second one the distance between the center of two consecutive bands and the third one the width of the bands. It is to be noted that the bands will overlap if the third number is greater than the second one. The three tables give the same quantities in the same order that is from left to right, the axial distance (X/D), the fitted value of the convection velocity on the wake axis (V_O/V_∞), the fitted value of the velocity wake width (r/D), the residual sum of squares (R.S.S.), the standard deviation of the fit (S.D.) and finally the number of measurements forming the radial profile (N).

TABLE A-I

NUMERICAL DATA RELATED TO THE FITS AT 7.6 TORR

(Combination: 60-30-30)

X/D	V_o/V_∞	r/D	R.S.S.	S.D.	N
60.0	0.144	2.01	9.8625E-3	2.0272E-2	26
90.0	0.103	3.75	2.2313E-2	2.6829E-2	33
120.0	0.110	2.16	8.8263E-3	1.5240E-2	40
150.0	0.090	2.68	1.3551E-2	1.8640E-2	41
180.0	0.095	2.35	1.0496E-2	1.6199E-2	42
210.0	0.082	2.37	8.1595E-3	1.2408E-2	55
240.0	0.066	2.83	8.5724E-3	1.2840E-2	54
270.0	0.072	2.10	5.5282E-3	1.0026E-2	57
300.0	0.058	2.89	1.1845E-2	1.4950E-2	55
330.0	0.054	3.37	1.0560E-2	1.3611E-2	59
360.0	0.055	2.43	5.9887E-3	1.1055E-2	51
390.0	0.053	2.23	6.5648E-3	1.1026E-2	56
420.0	0.048	2.35	3.5921E-3	8.9345E-3	47
450.0	0.043	2.42	6.3150E-3	1.0814E-2	56
480.0	0.042	2.67	5.5454E-3	1.0638E-2	51
510.0	0.037	2.94	4.1791E-3	8.7168E-3	57
540.0	0.036	2.81	3.2356E-3	8.6745E-3	45
570.0	0.036	2.51	3.0384E-3	8.5055E-3	44
600.0	0.039	2.51	8.2016E-3	1.3811E-2	45
630.0	0.034	2.48	1.5223E-3	6.0934E-3	43
660.0	0.033	2.86	1.8317E-3	7.3398E-3	36
690.0	0.037	2.33	1.6360E-3	6.5615E-3	40
720.0	0.028	3.54	1.4876E-3	7.5640E-3	28
750.0	0.030	2.77	4.6519E-4	5.2311E-3	19
780.0	0.031	3.36	5.9006E-4	6.7372E-3	15
810.0	0.025	3.84	8.0075E-4	7.5628E-3	16
840.0	0.022	3.21	1.3622E-4	3.6908E-3	12
870.0	0.024	3.84	4.9932E-4	6.7374E-3	13
900.0	0.019	6.55	2.9015E-4	4.9172E-3	14
930.0	0.020	4.26	2.8331E-4	4.4985E-3	16
960.0	0.018	4.13	1.4467E-4	3.3359E-3	15
990.0	0.023	3.05	1.8166E-4	4.7652E-3	10
1020.0	0.022	2.79	1.0384E-4	3.3967E-3	11
1050.0	0.019	3.94	1.3120E-4	3.3065E-3	14
1080.0	0.019	4.64	2.3215E-5	2.7818E-3	5
1110.0	0.017	5.38	1.3693E-4	4.4229E-3	9
1140.0	0.016	5.62	6.6355E-5	4.7030E-3	5

TABLE A-II

NUMERICAL DATA RELATED TO THE FITS AT 7.6 TORR

(Combination: 60-30-60)

X/D	V_o/V_∞	r/D	R.S.S.	S.D.	N
60.0	0.135	2.11	2.8948E-2	2.3824E-2	53
90.0	0.110	2.71	3.4095E-2	2.2229E-2	71
120.0	0.095	2.92	3.2624E-2	2.0719E-2	78
150.0	0.094	2.49	2.1482E-2	1.7154E-2	75
180.0	0.093	2.22	2.0313E-2	1.5739E-2	84
210.0	0.082	2.41	1.6671E-2	1.3686E-2	91
240.0	0.070	2.64	1.7161E-2	1.3035E-2	103
270.0	0.064	2.70	1.7435E-2	1.3204E-2	102
300.0	0.061	2.66	1.9393E-2	1.3463E-2	109
330.0	0.058	2.71	1.9382E-2	1.2816E-2	120
360.0	0.056	2.52	1.6272E-2	1.2163E-2	112
390.0	0.054	2.30	1.3721E-2	1.1220E-2	111
420.0	0.050	2.28	1.3159E-2	1.0791E-2	115
450.0	0.042	2.57	1.1986E-2	1.0036E-2	121
480.0	0.038	2.95	1.0635E-2	9.9234E-3	110
510.0	0.039	2.72	7.1661E-3	9.2919E-3	85
540.0	0.037	2.69	6.1890E-3	8.6877E-3	84
570.0	0.037	2.62	1.1362E-2	1.1113E-2	94
600.0	0.036	2.63	9.7111E-3	1.1087E-2	81
630.0	0.037	2.40	8.5319E-3	1.1285E-2	69
660.0	0.034	2.52	2.8741E-3	6.5496E-3	69
690.0	0.035	2.54	3.2279E-3	6.9410E-3	69
720.0	0.033	2.75	2.9156E-3	7.0901E-3	60
750.0	0.029	3.26	1.9411E-3	6.4265E-3	49
780.0	0.029	3.12	1.3563E-3	6.1380E-3	38
810.0	0.025	3.67	1.5321E-3	7.1463E-3	32
840.0	0.023	3.95	1.4022E-3	6.8366E-3	32
870.0	0.021	4.26	8.5957E-4	5.4443E-3	31
900.0	0.020	4.76	5.9212E-4	4.4427E-3	32
930.0	0.019	4.18	4.4690E-4	3.9256E-3	31
960.0	0.020	3.16	2.6506E-4	3.6405E-3	22
990.0	0.021	3.15	2.6564E-4	3.5566E-3	23
1020.0	0.023	2.93	2.1978E-4	3.8278E-3	17
1050.0	0.020	3.40	2.4871E-4	3.4414E-3	23
1080.0	0.014	4.69	9.8122E-5	2.6474E-3	16
1110.0	0.018	4.96	1.6548E-4	3.7135E-3	14
1140.0	0.017	5.41	2.0455E-4	4.1287E-3	14
1170.0	0.014	14.95	1.0063E-4	3.5466E-3	10

TABLE A-III

NUMERICAL DATA RELATED TO THE FITS AT 7.6 TORR

(Combination: 100-100-100)

X/D	V_o/V_∞	r/D	R.S.S.	S.D.	N
100.0	0.111	2.40	6.6469E-2	2.3342E-2	124
200.0	0.082	2.47	3.7477E-2	1.5401E-2	160
300.0	0.060	2.67	3.1353E-2	1.2983E-2	188
400.0	0.052	2.28	1.9919E-2	1.0730E-2	175
500.0	0.038	2.87	1.4343E-2	9.4978E-3	161
600.0	0.036	2.50	1.3040E-2	9.9018E-3	135
700.0	0.033	2.74	4.9423E-3	6.9953E-3	103
800.0	0.026	3.43	2.3607E-3	6.5515E-3	57
900.0	0.021	4.24	1.2168E-3	5.1999E-3	47
1000.0	0.021	3.19	4.4170E-4	3.5525E-3	37
1100.0	0.017	5.02	3.0536E-4	3.3024E-3	30

APPENDIX B

This appendix contains only one table giving all the pertinent numerical values pertaining to the fits of the radial profiles of the convection velocity at 20 torr (54 torr-inches). The various quantities and symbols used in this appendix are described in appendix A.

TABLE B-I

NUMERICAL DATA RELATED TO THE FITS AT 20 TORR

(Combination: 60-30-60)

X/D	V_o/V_∞	r/D	R.S.S.	S.D.	N
60.0	0.157	1.87	2.4788E-3	1.5744E-2	12
90.0	0.168	1.68	4.3626E-3	1.4769E-2	22
120.0	0.163	1.63	9.0895E-3	1.8348E-2	29
150.0	0.147	1.74	1.3989E-2	1.9392E-2	37
180.0	0.140	1.73	1.8414E-2	1.9002E-2	53
210.0	0.115	1.90	2.5483E-2	1.9358E-2	70
240.0	0.106	1.84	2.2261E-2	1.6894E-2	80
270.0	0.111	1.68	1.7392E-2	1.4653E-2	83
300.0	0.099	1.75	1.7834E-2	1.5219E-2	79
330.0	0.087	1.80	1.9884E-2	1.4947E-2	91
360.0	0.078	1.88	1.5048E-2	1.2931E-2	92
390.0	0.070	2.10	9.0451E-3	9.8620E-3	95
420.0	0.062	2.35	1.3403E-2	1.1695E-2	100
450.0	0.054	2.46	1.3713E-2	1.1769E-2	101
480.0	0.049	2.51	1.0039E-2	1.0019E-2	102
510.0	0.049	2.47	8.7003E-3	1.0177E-2	86
540.0	0.052	2.28	8.8248E-3	1.0311E-2	85
570.0	0.048	2.65	9.5620E-3	1.0799E-2	84
600.0	0.043	2.91	8.2114E-3	9.4992E-3	93
630.0	0.047	2.36	8.3771E-3	9.5423E-3	94
660.0	0.046	2.33	1.1595E-2	1.1226E-2	94
690.0	0.041	2.68	8.7578E-3	1.1029E-2	74
720.0	0.039	2.91	6.3815E-3	9.7594E-3	69
750.0	0.038	2.95	4.9787E-3	8.7519E-3	67
780.0	0.033	3.34	4.3985E-3	8.1024E-3	69
810.0	0.033	3.08	4.2721E-3	7.9262E-3	70
840.0	0.035	2.82	3.3159E-3	7.6950E-3	58
870.0	0.036	2.64	2.6702E-3	7.4585E-3	50
900.0	0.035	2.71	1.8965E-3	6.2857E-3	50
930.0	0.032	3.23	1.5572E-3	5.6957E-3	50
960.0	0.032	3.50	1.2908E-3	6.0729E-3	37
990.0	0.032	3.44	1.4303E-3	6.4859E-3	36
1020.0	0.029	3.62	8.3188E-4	5.4507E-3	30
1050.0	0.030	3.45	6.9908E-4	5.5132E-3	25
1080.0	0.033	2.93	5.1690E-4	4.9613E-3	23
1110.0	0.030	3.27	3.7867E-4	5.2008E-3	16
1140.0	0.027	3.75	3.5112E-4	4.6846E-3	18
1170.0	0.028	3.86	3.9720E-4	6.0091E-3	13
1200.0	0.035	2.64	2.2592E-4	5.3141E-3	10